ELSEVIER

Journal of Fluids and Structures 24 (2008) 527–540

JOURNAL OF FLUIDS AND STRUCTURES

www.elsevier.com/locate/jfs

Fluid–structure interaction between a two-dimensional mat-type VLFS and solitary waves by the Green–Naghdi theory

D. Xia[a], R.C. Ertekin[b,*], J.W. Kim[c]

[a]*INTEC Engineering Partnership Ltd., 15600 JFK Blvd, Houston, TX 77032, USA*
[b]*Department of Ocean and Resources Engineering, University of Hawaii, 2540 Dole St., Holmes Hall 402, Honolulu, HI 96822, USA*
[c]*Technip USA, 11700 Old Katy Rd., Suite 150, Houston, TX 77079, USA*

Received 1 June 2007; accepted 22 October 2007
Available online 7 January 2008

Abstract

The two-dimensional, nonlinear hydroelasticity of a mat-type very large floating structure (VLFS) is studied within the scope of linear beam theory for the structure and the nonlinear, Level I Green–Naghdi (GN) theory for the fluid. The beam equation and the GN equations are coupled through the kinematic and dynamic boundary conditions to obtain a new set of modified GN equations. These equations represent long-wave motion beneath an elastic plate. A set of jump conditions that are necessary for the continuity (or the matching) of the solutions in the open water region and that under the structure is derived through the use of the postulated conservation laws of mass, momentum, and mechanical energy. The resulting governing equations, subjected to the boundary and jump conditions, are solved by the finite-difference method in the time domain. The present model is applicable, for example, to the study of the hydroelastic response of a mat-type VLFS under the action of a solitary wave, or a frontal tsunami wave. Good agreement is observed between the model results and other published theoretical and numerical predictions, as well as experimental data. The results show that consideration of nonlinearity is important for accurate predictions of the bending moment of the floating elastic plate. It is found that the rigidity of the structure greatly affects the bending moment and displacement of the structure in this nonlinear theory.

Keywords: Green–Naghdi equations; Hydroelasticity; Mat-type VLFS; Solitary waves; Nonlinear shallow-water waves; Bending moment

1. Introduction

A very large floating structure (VLFS) with a 'small' draft behaves like an elastic plate. The frontal wave of a tsunami around a VLFS can be described as a solitary wave. In this work, we consider a thin elastic plate under the action of a solitary wave in shallow water to investigate the dynamic response of a VLFS to a tsunami.

Stoker (1957) studied long waves beneath a floating elastic plate first by focusing his attention on the transmission of waves beneath a floating breakwater, within the scope of linear wave theory. His work has been extended to three

*Corresponding author. Tel.: +1 800 956 6818; fax: +1 800 956 3498.
E-mail addresses: Dingwu.Xia@intec-hou.com (D. Xia), ertekin@hawaii.edu (R.C. Ertekin), JWKim@Technip.com (J.W. Kim).

0889-9746/$ - see front matter © 2007 Elsevier Ltd. All rights reserved.
doi:10.1016/j.jfluidstructs.2007.10.009

dimensions by Evans and Davies (1968). Forbes (1986, 1988) investigated two-dimensional periodic waves beneath an elastic plate resting on the surface of an infinitely deep fluid, by use of a high-order series expansion technique. Lu (1991) examined the transmission and reflection of a soliton by a two-dimensional structure. He used the matched asymptotic-expansion method which gives a relation between the outer solution governed by the Boussinesq equations and the inner solution governed by the Laplace equation. Takagi (1996, 1997) derived the Boussinesq-class equations which represent a long-wave motion beneath an elastic plate, and the matching conditions between the ordinary and the modified Boussinesq equations by employing the matched asymptotic-expansion method. Ertekin and Kim (1999) studied the hydroelastic behavior of a three-dimensional mat-type VLFS in oblique waves by use of the linear Green–Naghdi (GN) theory.

In the present work, the Level I GN equations that represent long-wave motion beneath an elastic plate are derived, and the matching conditions are developed by employing a set of jump conditions. The theory and the numerical method used are discussed in Sections 2 and 3, respectively. Results, the importance of various parameters of the problem, and comparisons with the available experimental data are provided in Section 4.

2. Theory

The coordinate system and geometry of the fluid–structure system of the two-dimensional problem are depicted in Fig. 1. The beam is taken from a strip of unit width from a plate of large aspect ratio (beam length over beam width ratio is large). The beam is envisioned as the strip of a floating runway that freely floats on the top of Region II, with a draft d length b and thickness h_p. In Fig. 1, m is the mass per unit length of the beam (that is, of unit width). Its thickness is much smaller than its length so that the Kirchhoff thin-plate theory can be applied. The wave propagates parallel to the beam-length direction so that the hydroelastic phenomenon also is two-dimensional.

The whole domain is divided into three parts. Regions I and III contain the ordinary shallow-water wave problems. A nonlinear, long (solitary) wave comes from left and excites the motion of the beam. The inviscid fluid motion is assumed to be governed by the Level I GN theory [see, e.g., Ertekin and Wehausen (1986)]. The sea floor is flat. The still-water depth in the open water area is h_0, and in Region II, it is $h_0 - d$. We further assume that the runway is horizontally restrained somehow, and thus, no horizontal motion in the x direction is allowed.

2.1. Governing equations

The governing equations for the motion of the fluid are provided by the Level I GN theory [see, e.g., Green and Naghdi (1976)]. They can be written in a compact form [see, e.g., Ertekin and Becker (1998)]:

$$\eta_t + \frac{\partial[(h+\eta)u]}{\partial x} = 0, \tag{1}$$

$$\dot{u} + g\eta_x + \frac{\hat{p}_x}{\rho} = -\frac{1}{6}[4\eta_x\ddot{\eta} + 2(h+\eta)(\ddot{\eta})_x], \tag{2}$$

where ρ is the mass density of water, $\hat{p}$ is the pressure on the upper surface of water, and η is the surface displacement, and $u(x,t)$ is the horizontal velocity of fluid particles in the x direction. The subscripts, x and t, denote the partial derivatives, g is the gravitational acceleration, h the still water depth, and equals to h_o in Regions I and III, and to h_1 in Region II. The superposed dot denotes the material derivative, i.e., $\dot{\eta} = \eta_t + u(\partial\eta/\partial x)$. When there is no plate floating on the top of the fluid surface, the atmospheric pressure, $\hat{p}$, is set to zero. In Region II, however, $\hat{p}$ equals to the pressure on the bottom of the plate, while the atmospheric pressure on the top of the plate is set to zero.

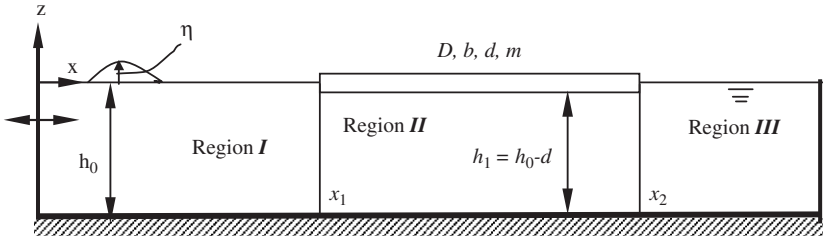

Fig. 1. Definition sketch of the problem.

It is noted that the integrated pressure through the water column, in the Level I GN theory, is given by [see, e.g., Ertekin (1984)]

$$P = \tfrac{1}{6}\rho(h+\eta)^2(2\ddot{\eta}+3g) + \hat{p}(h+\eta). \tag{3}$$

Since we are considering long waves, the linear beam theory is applied to the structure, i.e.,

$$m\eta_{tt} + D\eta_{xxxx} + mg = \hat{f}, \tag{4}$$

where $\hat{f}$ is the force acting by water on the bottom of plate, i.e., $\hat{p}$ times the width of the beam, D is the flexural rigidity of the plate, and is defined by $D = Eh_p^3/[12(1-v^2)]$, and E and v are Young's modulus and Poisson's ratio of the plate, respectively. It is noted that the dimension of each term in Eq. (4) is force/length since we are considering a beam of unit width.

The motion of the fluid and the plate is coupled through the dynamic free-surface condition. We also assume that the displacement of the plate and the fluid-surface elevation under the bottom of the plate are the same, i.e., no air gap is allowed.

After we substitute $\hat{f}$ from Eq. (4) into Eq. (2), and use the fact that the continuity equation is the same as in Eq. (1), except for the fluid sheet thickness, we can obtain the governing equations for the fluid–plate Region II:

$$\eta_t + \frac{\partial[(h_1+\eta)u]}{\partial x} = 0, \tag{5}$$

$$\dot{u} + g\eta_x + \frac{(m\eta_{tt} + D\eta_{xxxx} + mg)_x}{\rho} = -\frac{1}{6}[4\eta_x\ddot{\eta} + 2(h_1+\eta)(\ddot{\eta})_x]. \tag{6}$$

Eqs. (5) and (6) are the new, modified Level I GN equations (two-dimensional) that are nonlinear.

2.2. Initial and boundary conditions

We assume that there are waves initially ($t = 0$) and they are at a distance away from the plate. The velocities and surface elevation are initially set according to the analytical solution of a solitary wave that the Level I GN theory provides [see, e.g., Ertekin (1984)]. The piston wave-maker generates waves by having its velocity specified such that the generated waves are consistent with the initial wave inside the domain. In the solitary-wave case, the up-stream boundary becomes an open boundary after the entire wave enters the domain.

The downstream boundary is an open boundary. The open boundary condition used there is the Orlanski condition,

$$\frac{\partial\Omega}{\partial t} \pm c\frac{\partial\Omega}{\partial x} = 0, \tag{7}$$

where Ω could be η or u, and c is the phase velocity of the waves at the numerical boundaries. The minus sign denotes the left boundary and the plus sign the right boundary.

At the ends of the plate, free-free end boundary conditions of the beam require the vanishing of the bending moment and shear force. Thus, we have

$$D\eta_{xx} = D\eta_{xxx} = 0 \quad \text{at } x = x_1^+ \text{ and } x_2^-. \tag{8}$$

Since we assume that there is no gap between the bottom surface of the beam and the top surface of the fluid layer, the fluid under the tip of the beam should also satisfy the conditions given by Eq. (8). Because $\eta_{xx}|_{x_i} = 0$ and $\eta_{xxx}|_{x_i} = 0$ ($i = 1, 2$) at any time t, $\eta_{xxt}|_{x_i} = 0$ and $\eta_{xxxt}|_{x_i} = 0$ should be satisfied for all t. By taking the second- and third-order derivatives about x on both sides of the mass continuity equation, Eq. (5), we obtain the boundary conditions (at $x = x_i, i = 1, 2$) for the fluid motion under the ends of the beam as

$$3\eta_x u_{xx} + (h+\eta)u_{xxx} = 0, \tag{9}$$

$$4\eta_x u_{xxx} + (h+\eta)u_{xxxx} + \eta_{xxxx}u = 0. \tag{10}$$

2.3. Jump conditions

In the following formulation, only the left side of the elastic plate is treated here because the solution for the other side is obtained by employing the same technique.

The appropriate jump conditions are demanded by the theory because the fluid surface is discontinuous at the juncture of Regions I and II, $x = x_1^{\pm}$. Here, the plus sign denotes the limit approaching from the right toward x_1, while the minus sign from the left toward x_1. The jump conditions are necessary for having the mass, momentum, and mechanical energy flux at $x = x_1^{\pm}$ conserved.

Naghdi and Rubin (1981) provided a set of jump conditions for a flat bottom and steady motion by use of the conservation laws and when there is a rigid body floating on the fluid surface. Naghdi and Rubin (1981), and also Green and Naghdi (1986), applied them to a steady-flow problem. However, they additionally required the continuity of the surface elevation and surface pressure, $\hat{p}$, or the slope of the surface. In the present study, we cannot avoid discontinuities in the surface elevation and pressure since the motion of the elastic beam is relative at $x = x_1^-$ and x_1^+.

Based on the conservation of mass, momentum, director momentum (moment of vertical momentum), and mechanical energy (Naghdi and Rubin, 1981), the jump conditions for the case of a floating, elastic body are derived here. We assume the singularity to be stationary in the horizontal plane and identify the fixed location of the discontinuity by the vertical line at $x = x_1$. The sea bed is also assumed to be stationary in the present derivation, although this is not necessary in general.

By use of Leibnitz's rule, and by following Naghdi and Rubin (1981), the corresponding jump conditions for mass, horizontal and vertical momentum, director momentum, and energy conservation can be derived:

$$[[\rho\phi u]] = 0 \quad \text{at } x = x_1, \tag{11}$$

$$[[\rho\phi u(u\mathbf{e}_1 + \tfrac{1}{2}w\mathbf{e}_3) + P\mathbf{e}_1]] = \mathbf{F} \quad \text{at } x = x_1, \tag{12}$$

$$[[\tfrac{1}{12}\rho\phi uw\mathbf{e}_3]] = \mathbf{L} \quad \text{at } x = x_1, \tag{13}$$

$$[[\tfrac{1}{2}\rho\phi u(u^2 + \tfrac{1}{3}w^2 + g\psi) + Pu]] = \mathbf{F}\cdot\mathbf{V} + \mathbf{L}\cdot\mathbf{W} \quad \text{at } x = x_1, \tag{14}$$

where $\mathbf{e}_i (i = 1, 3)$ are the unit base vectors corresponding to the x and z axes, respectively, ϕ is the thickness of the fluid sheet, $w = \dot{\phi}$ is the vertical velocity of the water column, and ψ the mid-position of the fluid sheet, i.e., $\psi = (-h_0 + \eta)/2$ and $\psi = (-h_0 - d + \eta)/2$ in the regions without and with the plate, respectively.

In the jump conditions above, we use the notation

$$[[f]] = f_+ - f_-, \tag{15}$$

to mean $f_+ = \lim_{x\to x_1^+} f, f_- = \lim_{x\to x_1^-} f$, i.e., the values of f on the sides $x = x_1^+$ and $x = x_1^-$ of the jump, respectively. Here, f can be any one of η, u, ϕ, w, P. We assume that at $x = x_1$, the value of f changes from f_- at $x = x_1^-$ to f_+ at $x = x_1^+$. And we define the following:

$$\mathbf{F} = \lim_{\delta\to 0}\int_{x_1-\delta}^{x_1+\delta} [\hat{p}\eta_x\mathbf{e}_1 + (\bar{p} - \hat{p})\mathbf{e}_3]\mathrm{d}x, \tag{16}$$

$$\mathbf{L} = \lim_{\delta\to 0}\int_{x_1-\delta}^{x_1+\delta} \left[-\frac{1}{2}(\bar{p} + \hat{p})\mathbf{e}_3\right]\mathrm{d}x, \tag{17}$$

$$\mathbf{F}\cdot\mathbf{V} = \lim_{\delta\to 0}\int_{x_1-\delta}^{x_1+\delta} [\hat{p}\eta_x u + (\bar{p} - \hat{p})w/2]\mathrm{d}x, \tag{18}$$

$$\mathbf{L}\cdot\mathbf{W} = \lim_{\delta\to 0}\int_{x_1-\delta}^{x_1+\delta} \left[-\frac{1}{2}(\bar{p} + \hat{p})w\right]\mathrm{d}x. \tag{19}$$

Eqs. (18) and (19) can be combined as

$$\mathbf{F}\cdot\mathbf{V} + \mathbf{L}\cdot\mathbf{W} = \lim_{\delta\to 0}\int_{x_1-\delta}^{x_1+\delta} -\hat{p}\phi_t\,\mathrm{d}x. \tag{20}$$

Also, from Eqs. (16) and (17), we obtain

$$\lim_{\delta\to 0}\int_{x_1-\delta}^{x_1+\delta} -\hat{p}\,\mathrm{d}x = \left(\frac{\mathbf{F}}{2} + \mathbf{L}\right)\cdot\mathbf{e}_3. \tag{21}$$

Substituting Eqs. (12) and (13) for **F** and **L** in Eq. (21), we obtain

$$\lim_{\delta\to 0}\int_{x_1-\delta}^{x_1+\delta} -\hat{p}\,\mathrm{d}x = \frac{\rho}{3}[[\phi uw]]. \tag{22}$$

When $x<x_1$, there is no plate, and thus $\hat{p}=0$. Therefore, Eq. (20) becomes

$$\begin{aligned}\mathbf{F}\cdot\mathbf{V}+\mathbf{L}\cdot\mathbf{W} &= \lim_{\delta\to 0}\int_{x_1-\delta}^{x_1+\delta} -\hat{p}\phi_t\,\mathrm{d}x = \lim_{\delta\to 0}\int_{x_1}^{x_1+\delta} -\hat{p}\phi_t\,\mathrm{d}x\\ &= -\phi_t|_{x_1^+}\lim_{\delta\to 0}\int_{x_1}^{x_1+\delta}\hat{p}\,\mathrm{d}x = \phi_t|_{x_1^+}\frac{\rho}{3}[[\phi uw]].\end{aligned} \tag{23}$$

In the case of energy conservation, Eq. (14), the factor, ϕu which is the mass flux through the matching intersection, is removed from all the terms without loss of any information. This makes the equation to have nonzero coefficients when the fluid is still. Eq. (14) then becomes

$$\left[\left[\frac{1}{2}\rho\left(u^2+\frac{1}{3}w^2+2g\psi\right)+\frac{P}{\phi}\right]\right] = \phi_t|_{x_1^+}\frac{\rho}{3}[[w]] \quad \text{at } x=x_1. \tag{24}$$

One can also derive a set of jump conditions similar to Eqs. (11)–(14) for the other jump point located at $x=x_2$.

3. Numerical scheme

Before discretizing the partial differential equations governing the motion of the fluid and the structure, i.e., Eqs. (1) and (2), in the open water, and Eqs. (5) and (6) where the structure is located, the time derivatives of η are removed by the application of the mass continuity equation, Eq. (1). This allows the governing equations to be decoupled, and an explicit time-stepping method can be used to solve the problem.

The fourth-order Runge–Kutta method is used to march in time. The second-order accurate central-difference formulas are used for the spatial derivatives. The mass continuity equation can be solved in a straight-forward manner. In the momentum equation, the time derivatives involve the spatial derivatives, e.g., u_t, u_{xt}, and u_{xxt}, which cannot be solved explicitly. These can be solved through a simultaneous set of linear equations inn two steps. To use the central-difference method for the derivatives of u at $x_1^{\pm}$, fictitious or ghost points are introduced on each side. To determine the numerical accuracy of the predictions, both the mass and the energy conservation were monitored in time. Moreover, to make the numerical scheme stable, the unwanted saw-tooth-oscillations of high wave frequency were removed by the use of a five-point filtering formula that Demirbilek and Webster (1992) used successfully.

4. Results and discussion

Based on the theory and the numerical procedure described above, the hydroelastic characteristics of a mat-type floating runway are investigated. The convergence and accuracy are discussed first. Then the model is verified by comparing the present results with the available numerical predictions and experimental data.

4.1. Convergence of the present scheme

In the convergence study, the computations were carried out for a beam with length $b=1\,\mathrm{km}$ and draft $d=5\,\mathrm{m}$. The nondimensional stiffness, $D/\rho g h^4$ is 3.2. The water depth is assumed to be 50 m. This physical model is similar to the one studied by Kashiwagi (1996), except that the length of the plate is assumed to be infinite in the present convergence study.

The computational domain is discretized into a number of intervals by the finite-difference grid. The convergence is tested by increasing the number of grid intervals on the beam. As an example, Fig. 2 shows the convergence of the maximum, absolute values of the displacement and bending moment along the structure for increasing number of grid intervals, N. The maximum value is taken at each grid of the plate for the whole process when the solitary wave passes through the plate. It is obvious that the maximum response converges uniformly as the number of grid intervals increases.

4.2. Verification of the present method

To test the validity of the present theory and its numerical implementation, comparisons are first made with the experimental data of Liu et al. (1998). In their experiments, they use a wave-maker at the left-side boundary. In the

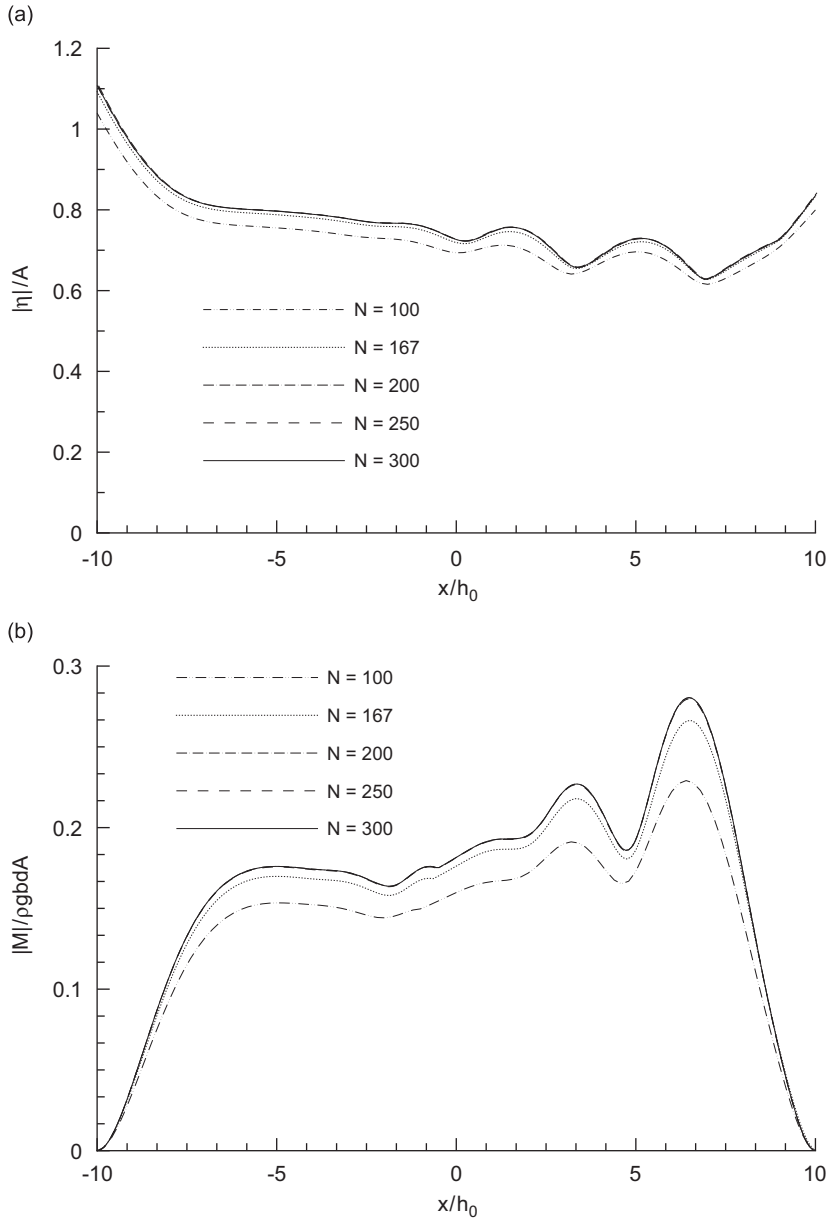

Fig. 2. Convergence of the maximum response along the beam for $A/h_0 = 0.3$, $D/\rho g h_o^4 = 3.2$. (a) Displacement and (b) bending moment.

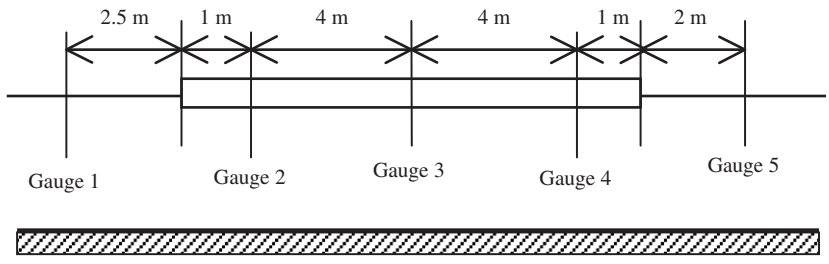

Fig. 3. Locations of the wave gauges.

present work, the generation of the solitary wave is different. We use the exact, analytical solitary-wave solution [see, e.g., Ertekin (1984)] of the Level I GN equations to specify the initial velocity and surface elevation.

The experimental structure used a 10 m long and 20 mm thick polyethylene plate with a modulus of elasticity of around 950 MPa, density of 0.914 kg/m^3 and Poisson's ratio of 0.3. The water depth in the experiments was 0.4 m. The incoming solitary wave was from the left side, and its amplitude, A, defined as the height from the still-water level to its peak was 0.04 m. There were five wave gauges (Fig. 3): one in upstream open water (Gauge 1), three in region II (Gauges 2–4), and one in the downstream open region (Gauge 5), as shown in Fig. 3.

The values of the corresponding nondimensionalized flexural rigidity and solitary-wave amplitude are the following: $D/\rho g h_o^4 = 2.77$ and $A/h_o = 0.1$, respectively. To match the phase of the solitary wave in the experiments, results in the

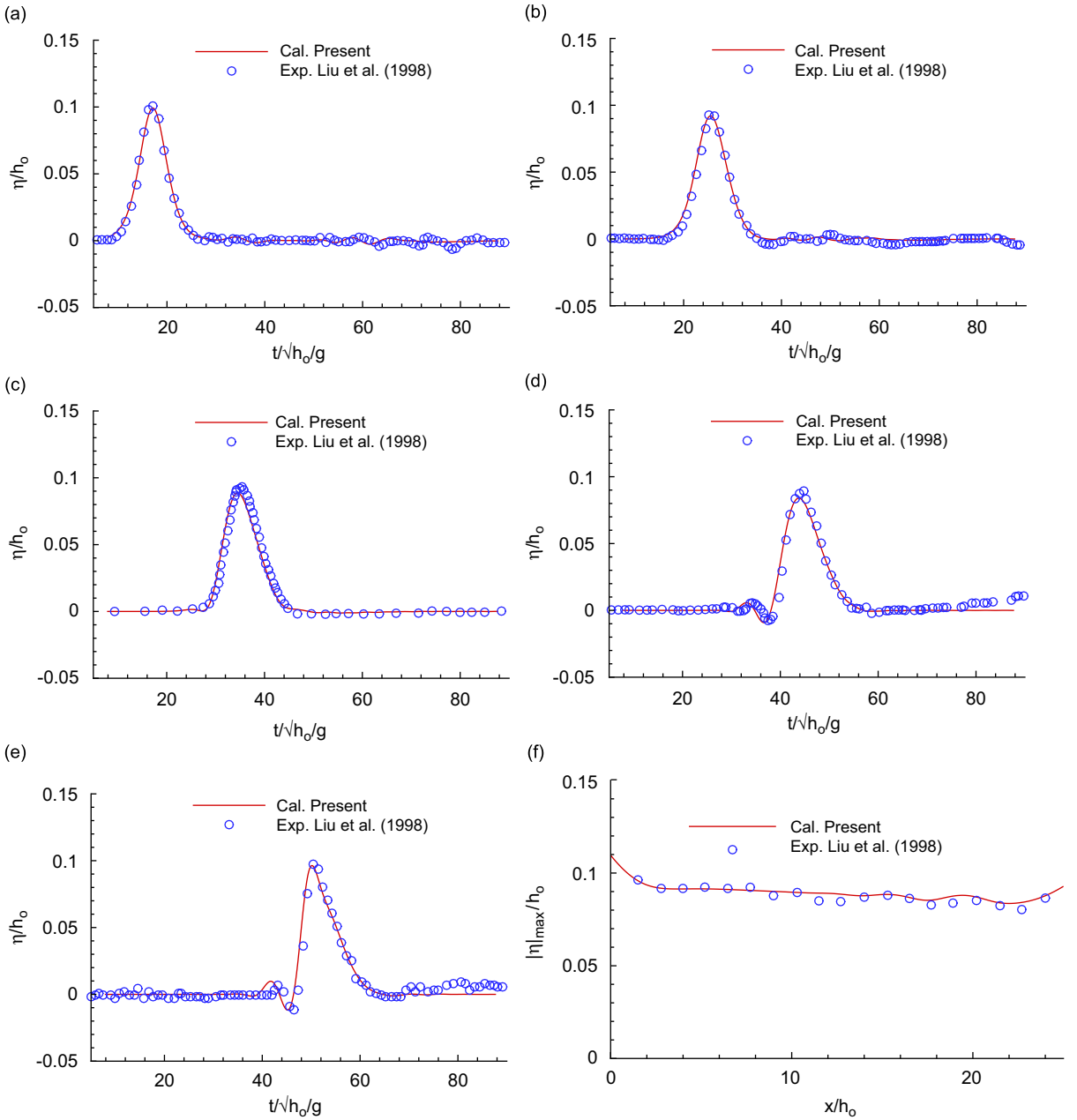

Fig. 4. Comparison of the experimental data with the present results for $A/h_0 = 0.1$, $D/\rho g h_o^4 = 2.37$. (a) Gauge 1, (b) Gauge 2, (c) Gauge 3, (d) Gauge 4, (e) Gauge 5, and (f) maximum displacement of the structure.

present calculations are shifted so that both peaks occur at the same time. This is also done for the other cases discussed in this section.

In Fig. 4, we present a comparison of our results and experimental data of Liu et al. (1998) for free-surface elevation and structural deformation. Figs. 4(a)–(e) show the comparisons of the time history of the surface elevation (Regions I and III) or structural displacements (Region II) recorded at the wave gauges. The incoming wave profile in Fig. 4(a) shows good agreement with data. Figs. 4(b)–(d) show the comparison of the experimental data and present calculations for the plate displacement. Fig. 4(e) shows the free-surface elevation at the downstream wave gauge. The present calculations and measured data agree well on the plate and in the open water, and the largest difference occurs at the downwave side of the plate. End effects and flow separation (vortex shedding) in the experiments cannot be modeled in the present study.

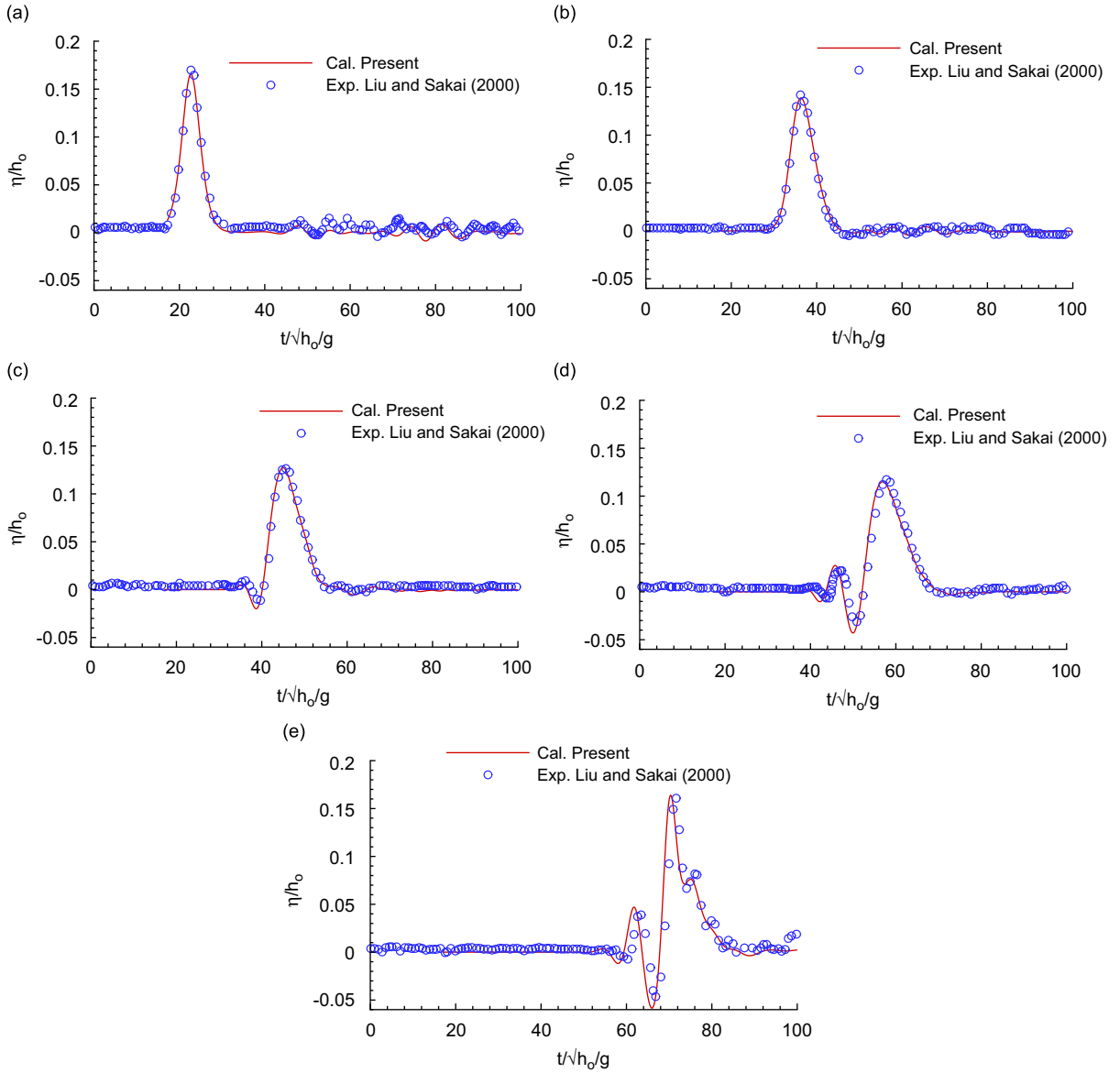

Fig. 5. Comparison of the experimental data with the present results for $A/h_0 = 0.167$, $D/\rho g h_o^4 = 5.07$. (a) Gauge 1, (b) Gauge 2, (c) Gauge 3, (d) Gauge 4, and (e) Gauge 5.

As a second comparison, we now consider the experimental data of Liu and Sakai (2000) in Fig. 5. The experimental study used a polyethylene plate with length $b = 10\,\text{m}$, mass density $\rho_s = 0.914\,\text{kg/m}^3$, $v = 0.3$, and $E = 550\,\text{MPa}$. The displacement and surface elevation were measured along the centerline of the flume. And $d = 0.02\,\text{m}$, $h_o = 0.3\,\text{m}$, and $A = 0.05\,\text{m}$. The wave gauge positions are the same as in Fig. 3, but distances are different: G_1 is 3 m from the upstream tip, G_2, G_3, and G_4 are in Region II and are 1.5, 4.5, and 8.5 m from the upstream tip, respectively, and G_5 is 3 m from the downstream plate edge in the open water.

Fig. 5(a) shows results of the comparison for the incoming wave. The free-surface profile and its peak are matched well, including the small tails representing reflected and radiated waves by the structure. The plate displacement and the downwave open water free-surface elevation agree well in general (Figs. 5(b)–(e)).

The solitary wave could not maintain its shape and speed when it enters into the plate–fluid region. This phenomenon can be observed in Figs. 5(c) and (d), and in Fig. 4(d), where dispersion and nonlinearity are no longer balanced. This is why the smaller leading waves occur. When relative stiffness becomes larger, such waves appear earlier.

The kinematics and the pressure on the VLFS for the G–N solution are presented next. However, there is no experimental data available for comparison. Particle velocities at the water surface in both horizontal and vertical directions, i.e., u and w, respectively, are shown in Fig. 6. The snap shots in Figs. 6(a)–(d) correspond to the time of the surface elevation peak at Gauges 1–4, respectively. The dynamic pressure acting on the VLFS is presented in Figs. 7(a)–(c) at the time of the surface elevation peak at Gauges 2–4, respectively.

4.3. Comparison with the solutions of the Boussinesq equations

The present results are compared in Figs. 8 and 9 with the results of Takagi (1997) who used the Boussinesq equations [see, e.g., Wu (1981)] in shallow water, and linear beam theory with the inertial term for the structure neglected.

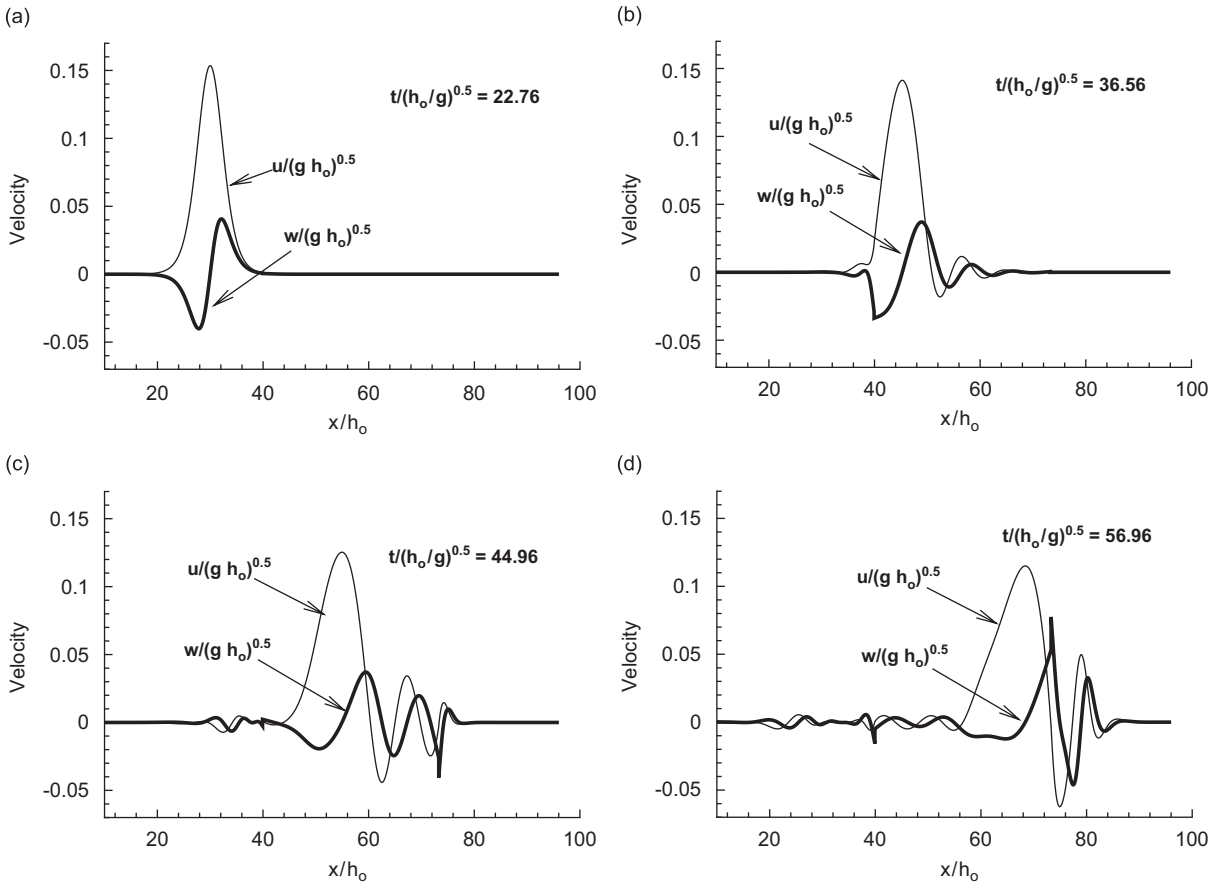

Fig. 6. Snap shots of the present calculated particle velocity at the water surface for $A/h_0 = 0.167$, $D/\rho g h_o^4 = 5.07$.

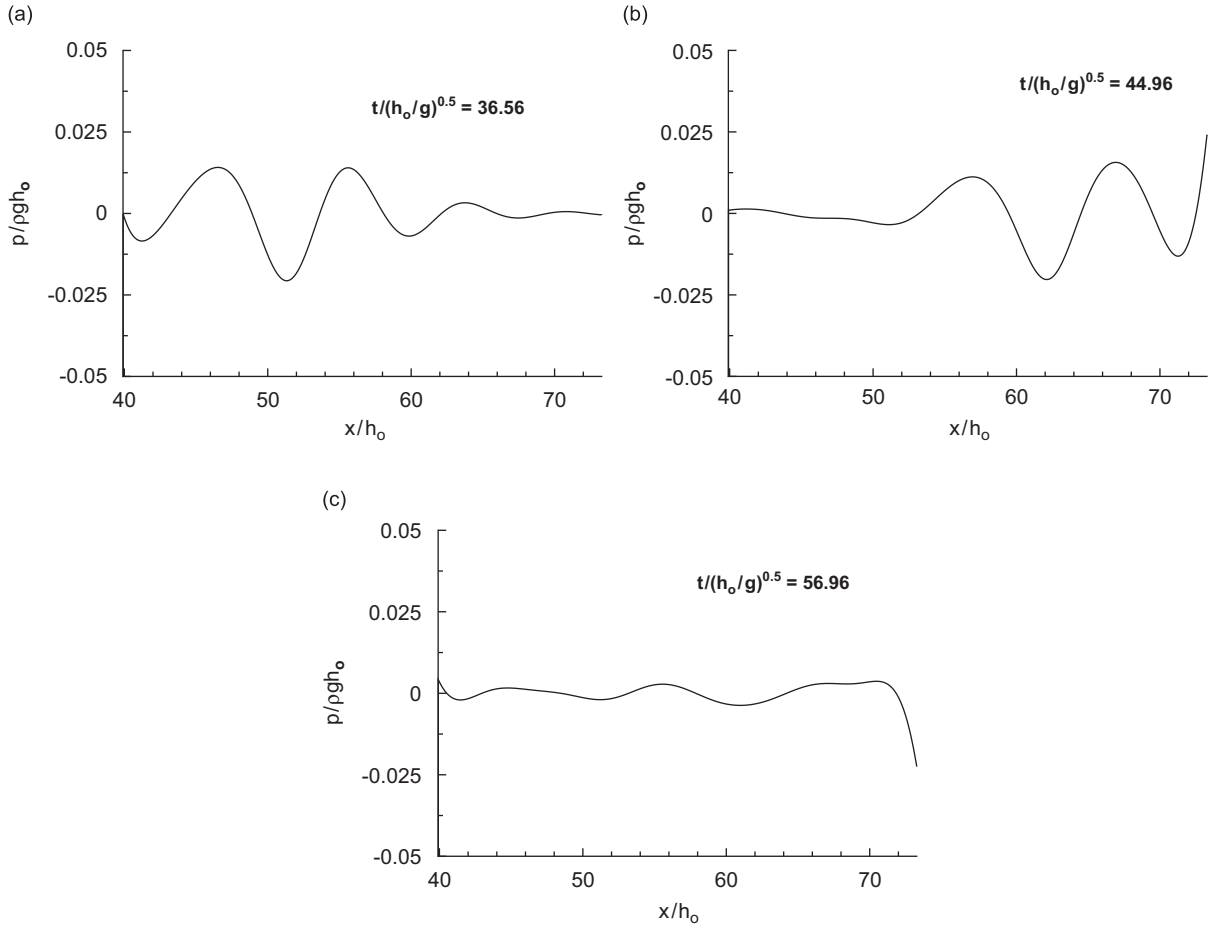

Fig. 7. Snap shots of pressure on the VLFS for $A/h_0 = 0.167$, $D/\rho g h_o^4 = 5.07$.

In this comparison, we have used $b/h_o = 7.30$, $D/\rho g h_o^4 = 3.33$ [rather than $D/\rho g h_o^4 = 1.11$ as in Takagi (1997)[1]], $d/h_o = 0.3$, $A/h_o = 0.2$. The solitary wave is propagating from right to left. The time series of the free-surface elevation and the beam displacement are compared for $\Delta t/(h_o/g)^{0.5} = 0.0005$ and $\Delta x/h_o = 0.06$.

Good agreement is observed at small time values. At large time values, however, the discrepancy becomes more apparent, especially for the higher solitary-wave amplitude ($A/h_o = 0.4$) case in Fig. 9. This is because of the use of different theories. The theoretical solitary-wave profile in the GN theory is wider than that obtained from the Boussinesq equations (Ertekin, 1984; Ertekin and Wehausen, 1986). In addition, different matching schemes are used. In the laboratory data, small oscillations occur in the open water region near the upstream end of the beam. This is seen in the results of Takagi (1997) in Figs. 8(b) and (c) and in Figs. 9(b) and (c), but this kind of oscillation does not appear in the present calculations. The agreement with data is generally better for small wave amplitudes where the oscillations are less.

4.4. *Effects of stiffness and nonlinearity*

The effects of the beam stiffness and nonlinearity of the solitary wave on the hydroelastic response of the same runway considered in Section 4.1 are further studied. A comparison of the maximum displacement and bending moment acting on the beam for various stiffnesses is shown in Figs. 10(a) and (b). The solitary-wave amplitude is $A/h_o = 0.2$, and the nondimensional stiffness, $D/\rho g h^4$, values are 0.8, 3.2, and 12.8.

The results show that the displacement and bending moment depend on the stiffness, such that, as nondimensional stiffness increases, the displacement decreases, while the bending moment increases. The stiffness does not significantly

[1]We thank Prof. Takagi for pointing out the correct stiffness used by him.

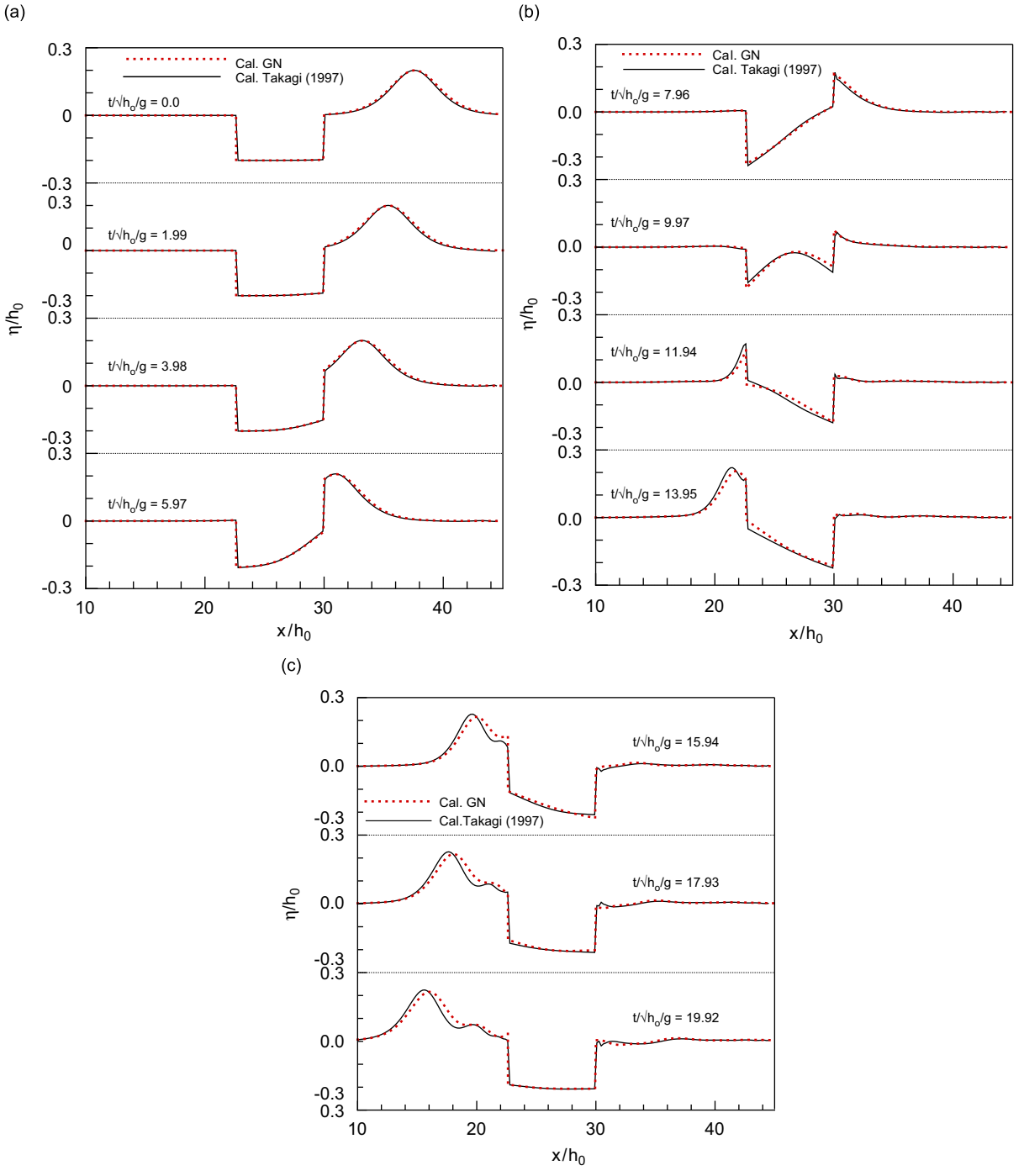

Fig. 8. Comparison of the present results with the solutions of the Boussinesq equations for $A/h_0 = 0.2$, $D/\rho g h_o^4 = 3.33$.

affect the maximum displacement in the upstream tip area. This is because a stiffer plate or structure can provide a larger reaction force to resist a change in its shape, and a softer structure is easier to move with the fluid surface.

The maximum hydroelastic response of the structure is shown in Fig. 11 for different wave amplitudes. A solitary wave of small amplitude induces larger relative displacements (note that in Fig. 11 wave amplitude is used in the normalization). Bending moments decrease with wave amplitude. The responses for $A/h_0 = 0.1$ and 0.4 are different. This shows that the nonlinearity becomes increasingly important for larger waves.

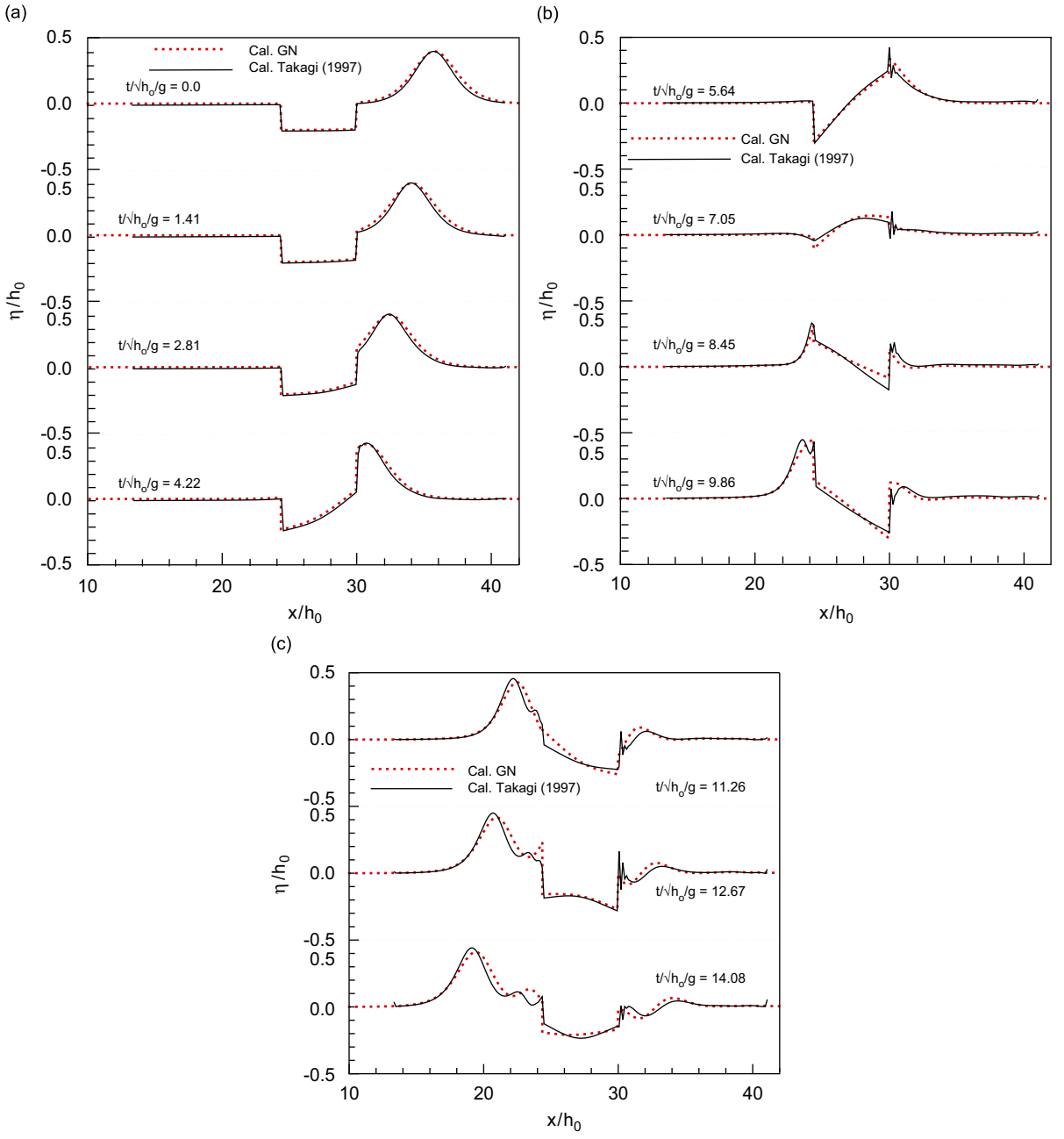

Fig. 9. Comparison of the present results with the solutions of the Boussinesq equations for $A/h_0 = 0.4$, $D/\rho g h_o^4 = 3.33$.

5. Conclusions

A modified set of Level I GN equations that represent a long wave beneath an elastic plate have been derived. Jump conditions are enforced in the solution of the governing equations. The solutions of the ordinary GN equations in the open water region and that of the modified GN equations under the structure are obtained by a finite-difference method. Numerical results showing the behavior of a solitary wave beneath an elastic plate are presented and compared with the existing predictions and experimental data. These results demonstrate that the nonlinearity of the fluid motion

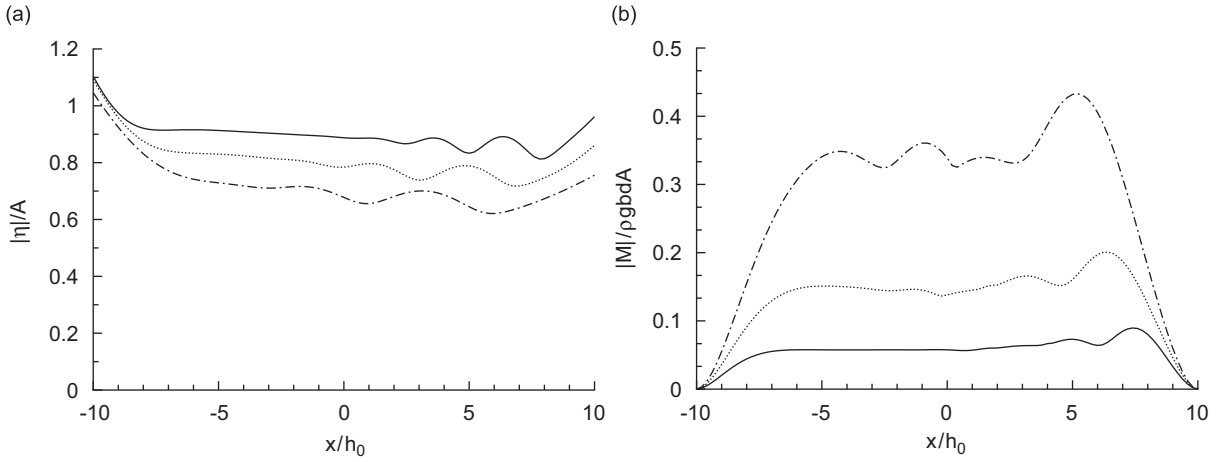

Fig. 10. Maximum response for different stiffness values and for $A/h_0 = 0.2$: $D/\rho g h_o^4 = 0.8$ —; $D/\rho g h_o^4 = 3.2 \ldots$; $D/\rho g h_o^4 = 12.8$–·–. (a) Displacement and (b) bending moment.

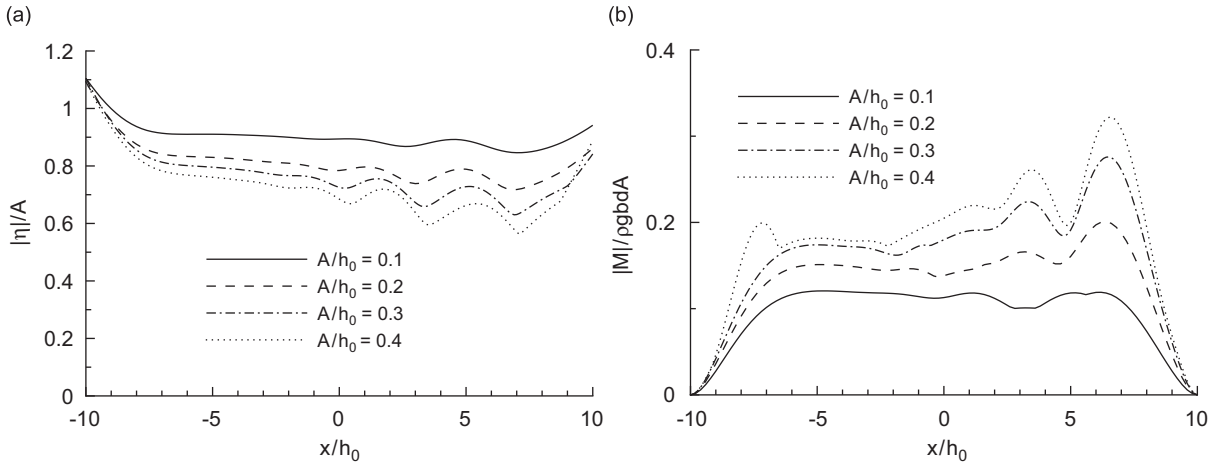

Fig. 11. Maximum response along the beam for various solitary-wave amplitudes and for $D/\rho g h_o^4 = 3.2$. (a) Displacement and (b) bending moment.

and the stiffness of the structure are important in the determination of the hydroelastic response of a VLFS to solitary waves. A particularly interesting feature of the results here is that, the more nonlinear the incoming wave is, the smaller the structural displacements are, but the larger the bending moments are.

Acknowledgments

This research is based originally upon work supported by ONR Grant no. N000149-81-0800 and by NSF Grant no. BES-9532037. The second author's (R.C.E.) work is partially supported by ONR Grant no. ONR N000140-21-0903.

References

Demirbilek, Z., Webster, W.C., 1992. Application of the Green–Naghdi theory of fluid sheets to shallow-water wave problems. Technical Report No. CERC-92-11, U.S. Army Corps of Engineers, Waterways Experiment Station, Vicksburg, MS, USA.

Ertekin, R.C., 1984. Soliton generation by moving disturbances in shallow water: theory, computation and experiment. Ph.D. Dissertation, University of California, Berkeley.

Ertekin, R.C., Becker, J.M., 1998. Nonlinear diffraction of waves by a submerged shelf in shallow water. ASME Journal of Offshore Mechanics and Arctic Engineering 120, 212–220.

Ertekin, R.C., Kim, J.W., 1999. Hydroelastic response of a mat-type structure in oblique, shallow-water waves. Journal of Ship Research 43, 241–254.

Ertekin, R.C., Wehausen, J.V., 1986. Some soliton calculations. In: Webster, W.C. (Ed.), Proceedings of 16th Symposium on Naval Hydrodynamics, Berkeley, July. National Academy Press, Washington, DC, pp. 167–184 (Discussion on p. 185).

Evans, D.V., Davies, T.V., 1968. Wave–ice interaction. Davidson Laboratory Report 1313, Stevens Institute of Technology, Hoboken, New Jersey.

Forbes, L.K., 1986. Surface waves of large amplitude beneath an elastic sheet. Part 1. High-order series solution. Journal of Fluid Mechanics 169, 409–428.

Forbes, L.K., 1988. Surface waves of large amplitude beneath an elastic sheet. Part 2. Galerkin solution. Journal of Fluid Mechanics 188, 491–508.

Green, A.E., Naghdi, P.M., 1976. A derivation of equations for wave propagation in water of variable depth. Journal of Fluid Mechanics 78 (Part 2), 237–246.

Green, A.E., Naghdi, P.M., 1986. A nonlinear theory of water waves for finite and infinite depths. Philosophical Transactions of the Royal Society of London. Series A 320, 37–70.

Kashiwagi, M., 1996. A B-spline Galerkin method for computing hydroelastic behaviors of a very large floating structure. In: Proceedings of Second International Workshop on VLFS. Ship Research Institute, Japan, pp. 149–156.

Liu, X., Sakai, S., 2000. Nonlinear analysis on the interaction of waves and flexible floating structure. In: Proceedings of 10th International Offshore and Polar Engineering Conference, Seattle, USA, pp. 101–108.

Liu, X., Sakai, S., Sasamoto, M., 1998. A numerical simulation for the interaction of mega float with solitary wave. In: Proceedings of 17th International OMAE Conference, CD-ROM: OMAE98-4343, 8pp.

Lu, Q.Q., 1991. The two-dimensional transmission and reflection of a solitary wave. Journal of Numerical Methods in Fluids 13, 1055–1070.

Naghdi, P.M., Rubin, M.B., 1981. On the transition to planing of a boat. Journal of Fluid Mechanics 103, 345–374.

Stoker, J.J., 1957. Water Waves. Interscience Publishers, Inc., New York.

Takagi, K., 1996. Interaction between tsunami and artificial floating island. In: Proceedings of International Offshore and Polar Engineering Conference, pp. 341–346.

Takagi, K., 1997. Interaction between solitary wave and floating elastic plate. ASCE Journal of Waterway, Port, Coastal, and Ocean Engineering 123, 57–62.

Wu, T.Y., 1981. Long waves in ocean and coastal waters. ASCE Journal of Engineering Mechanics 107, 501–522.